Available online at www.sciencedirect.com
ScienceDirect
Journal of Sound and Vibration 308 (2007) 287–301
JOURNAL OF SOUND AND VIBRATION
www.elsevier.com/locate/jsvi

Vibration analysis of micro-machined beam-type resonators

P.A. Hassanpour[a], W.L. Cleghorn[a,*], E. Esmailzadeh[b], J.K. Mills[a]

[a]*Department of Mechanical and Industrial Engineering, University of Toronto, Toronto, Ontario, Canada M5S 3G8*
[b]*Faculty of Engineering and Applied Science, University of Ontario Institute of Technology, Oshawa, Ontario, Canada*

Received 2 March 2007; received in revised form 25 May 2007; accepted 26 July 2007
Available online 4 September 2007

Abstract

This paper addresses the exact solution of the free vibrations of a beam subjected to an axial force and carrying a concentrated rotary mass along its length. The vibration problem is frequently encountered in the design and modeling of resonant double-ended tuning fork (DETF) micro-structures, where an exact model is needed to determine the natural frequencies of vibration as a function of design and operational parameters. The significance of the approach presented in this study is first to develop a model that includes all the contributing parameters and second that its solution has the ability to determine the exact mode shapes of vibration. These eigenvectors are necessary in the study of the time-domain response of resonators and also determine the stability regions for the operation of electrostatic comb-drive exciters/detectors. The effects of the axial force, location, mass ratio, and the radius of gyration on the natural frequencies and mode shapes of DETF are investigated. It has been shown that depending on the location of the concentrated mass, the inclusion of its rotary inertia may either decrease or increase the natural frequencies of the resonator compared with the case of no rotary inertia is included. In the case of designing a resonator to perform as a sensor, one can make use of the presented model to determine how the mass ratio, location and the radius of gyration can alter the sensitivity of the sensor in response to the input measurand.

1. Introduction

A resonator is a structure designed to vibrate at a specified frequency, usually one of its own natural frequencies. Micro-machined mechanical resonators are the building blocks of many MEMS devices combined such as the radio frequency filters and resonant sensors. The natural frequencies of a resonator are its key design parameters, which in turn, are functions of the inertia and the stiffness of that structure. The mass and the modulus of elasticity of a solid structure are stable and highly robust parameters that consequently, leads to the robustness and stability of the natural frequencies of that structure. Any slight variations in the natural frequency could even be used to determine some of the material properties such as the fatigue-life [1].

The stiffness of the structure is not only a function of its elasticity but also depends on the applied force, as the case of strings in tension. An applied force can alter the stiffness of the structure and hence, its natural

*Corresponding author.
E-mail address: cleghrn@mie.utoronto.ca (W.L. Cleghorn).

0022-460X/$ - see front matter © 2007 Elsevier Ltd. All rights reserved.
doi:10.1016/j.jsv.2007.07.043

Nomenclature

A	beam cross-sectional area
E	modulus of elasticity
I	area moment of the cross-sectional area of the beam
L_L	left side beam length
L_R	right side beam length
M	lumped mass
M_L	left side beam bending moment
M_R	right side beam bending moment
P	beam axial force
r	lumped mass radius of gyration
t	time
T	time function
V_L	left side beam shear force
V_R	right side beam shear force
W_L^*	left side beam deflection
W_R^*	right side beam deflection
x_L^*	left side beam abscissa coordinate
x_R^*	right side beam abscissa coordinate
Y_L^*	left side beam mode shape
Y_R^*	right side beam mode shape
η	dimensionless lumped mass radius of gyration
μ	dimensionless mass ratio
ξ	dimensionless mass location
ρ	density
σ	dimensionless axial force
ω	beam natural frequency
Ω	dimensionless beam natural frequency

frequencies. This feature will make the natural frequency a good candidate to be employed as a sensing mechanism, as in the case of resonant sensors. Measurands of interest, as an example being pressure and acceleration can be transformed into a force by using an intermediate mechanism. Thereafter, this force is applied to a resonator, which can be controlled to vibrate in its resonant frequency. In this way, the changes of natural frequency can be transformed into the changes of the measurand.

Beams are the widely used structure to act as resonators. Double-ended tuning forks (DETF) are one of the various beam-type resonators. A DETF consists of two parallel arranged clamped–clamped beams, as shown in Fig. 1. A two-sided comb-drive is attached to each beam to either excite or detect its vibration. In order to transmit the sensed force to the resonant beam, one clamped end is made free to move in the axial direction. With this set-up, the natural frequency of the beam can be varied by changing the axial force in the beam. The results obtained from the simulation of an electric circuit, which includes a DETF resonator, indicates that the

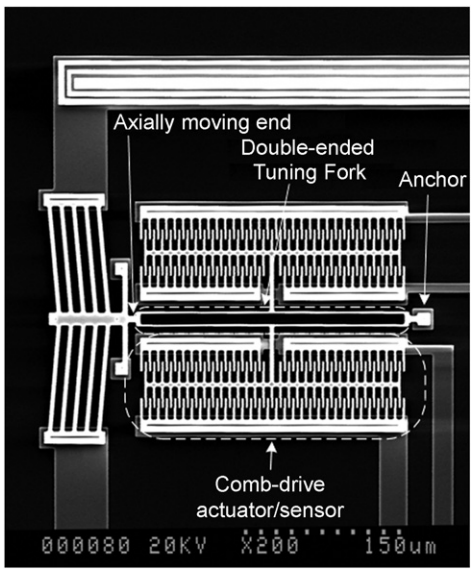

Fig. 1. Double-ended tuning fork with the comb-drive electrostatic excitation and detection mechanism. Each DEFT has two parallel clamped–clamped beams. The resonant sensor measures the force from the on-chip thermal actuator.

sensing output current of the resonator is proportional to the frequency at which it vibrates. Therefore, to achieve a higher signal to noise ratio in the output, it is desirable to design a resonator with higher natural frequencies.

In a recent study [2], the authors have shown that by placing the comb-drive at any location other than the mid-point of the clamped–clamped beams, the fundamental natural frequency will increase. In this case, the assumption of having a negligible rotary inertia for the comb-drive is no longer valid, because of the asymmetric configuration.

To find the natural frequencies of a beam, subjected to an axial force and having no attached concentrated mass, is a classical problem that has been solved for different combinations of the boundary conditions in the form of characteristic equations. In fact, vibration analysis of a beam is an initial condition boundary value problem, which can be transformed into an eigenvalue problem by using the method of separation of variables.

The application of this method is simple for a uniform beam having conventional boundary conditions. The problem becomes more complicated when a concentrated mass is attached to the beam. Chai and Low [3] used the Rayleigh's energy method to find the fundamental natural frequency of a slender uniform beam with a concentrated mass for two different boundary conditions of simply supported and clamped–clamped. Low and Chai [4] experimentally verified the analytical predictions of the Rayleigh's method for a clamped–clamped beam carrying a mass at its mid-point.

Low [5] determined the fundamental frequency of a vibrating beam carrying a concentrated mass at various locations. He utilized the Rayleigh's method with the trigonometric functions to study the effect of added masses and their locations on the natural frequency of beams. He introduced an equivalent-center method in which, the fundamental frequency of a beam carrying an off-center mass could be predicted by using the results associated with the center-loaded beams. De Rosa et al. [6] studied the dynamic behavior of a slender beam with a concentrated mass at an arbitrary abscissa. The beam in this study has elastic boundary conditions, which restrain the beam elastically against any rotations and translations at either ends. The result of their exact solution was compared with those from the approximate solutions.

Naguleswaran [7] investigated the frequency equations of that problem for all combinations of the conventional boundary conditions in the form of 4×4 determinants being equated to zero. Skrinar [8] developed a model for the vibration of a beam with a rotary mass within its interval. In this study, the efficacy of the model was demonstrated experimentally. Currie and Cleghorn [9] determined the fundamental vibration frequency of a uniform beam subjected to an axial tension. The beam in their study was taken as built-in at both ends and carried a concentrated mass attached to its mid-point. They assumed the beam had no rotation at its mid-point. An analytical solution was found for the natural frequencies, mode shapes and the orthogonality conditions of an arbitrary system of Euler–Bernoulli beams interconnected by arbitrary joints and been subjected to arbitrary boundary conditions [10].

In a recent study, the authors [2] modeled a micro-beam resonator as an Euler–Bernoulli beam subjected to an axial force and having a lumped mass attached to an intermediate point along the beam. They studied the effects of the attached mass, its location, and the axial force on the natural frequencies and mode shapes of vibration of the resonator. The modeling of the beam presented in Ref. [2] was expanded to model the MEMS device as shown in Fig. 1 [11].

In another study, the authors re-examined the model with the assumption that the concentrated mass is guided and having an infinite rotary inertia [12]. The practical design of the micro-beam resonators indicates that on one hand the rotary inertia of the lumped mass cannot be ignored, and on the other hand the rotary inertia cannot be assumed infinite. Moreover, if a resonant beam in the form of a comb-drive is either excited or its vibration is sensed, then it will be necessary to ensure that the motion of the comb-drive forks remains in the stable region [13]. This requirement necessitates the detailed study of the vibration of the resonator and its exact mode shapes.

In this paper, the deterministic vibration of a beam with a lumped mass at its interval is investigated. The effect of the rotary inertia of the lumped mass is included in the model. The beam is assumed to experience a quasi-static axial force. Moreover, the location of the attached lumped mass can be at any point along the beam. The methods of separation of variables and eigenvalue problem are used to derive the exact characteristic equation. Thereafter, the exact natural frequencies of vibration and their corresponding mode

shapes are evaluated. Although the approximate and energy methods, namely, Dunkerly and Rayleigh–Ritz, can give the natural frequencies of the resonator with enough accuracy, they cannot be used to predict the transient and the steady-state behavior of the resonator in the time domain. The reason being that in the Rayleigh–Ritz method, the assumed functions are only required to satisfy the geometrical boundary conditions, so it is admissible to take a function that does not represent the real mode shapes of the system even qualitatively.

2. Mathematical modeling

The schematic diagram for the model of a slender beam, subjected to an axial force P, and carrying an attached concentrated mass M along its length is shown in Fig. 2. The governing equations of motion of the beam, under axial force, could be written as [14]

$$\rho A\frac{\partial^2 W^*}{\partial t^2}+EI\frac{\partial^4 W^*}{\partial x^{*4}}-P\frac{\partial^2 W^*}{\partial x^{*2}}=0,\quad 0\leqslant x^*\leqslant L_L+L_R,\quad t>0. \tag{1}$$

The beam, shown in Fig. 2, can be treated as two separate beams connected to each other through the lumped mass. One can obtain the governing equations of motion for this system by investigating the dynamics of each separate beam, as shown in Fig. 3. In this figure, the reactions of the bending moments and shear forces of both beams on the limped mass are shown on its free diagram. In addition, the reactions due to the axial force are shown on the lumped mass. It can be shown that as these two reaction forces are assumed equal, unidirectional, and opposite, they have no contribution on the kinetics of the lumped mass [2]. By adopting two sets of coordinates originated at the location of the lumped mass, the dimensionless equations of motion for each beam are obtained as [2]:

For the left beam:

$$\frac{\partial^2 W_L}{\partial t_L^2}+\frac{\partial^4 W_L}{\partial x_L^4}-2P_L\frac{\partial^2 W_L}{\partial x_L^2}=0,\quad 0\leqslant x_L\leqslant 1,\quad t_L\geqslant 0, \tag{2}$$

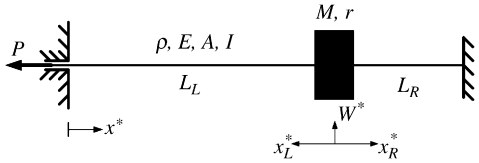

Fig. 2. A slender beam with a lumped mass within its interval under axial force. P is assumed positive when axial force is tensile.

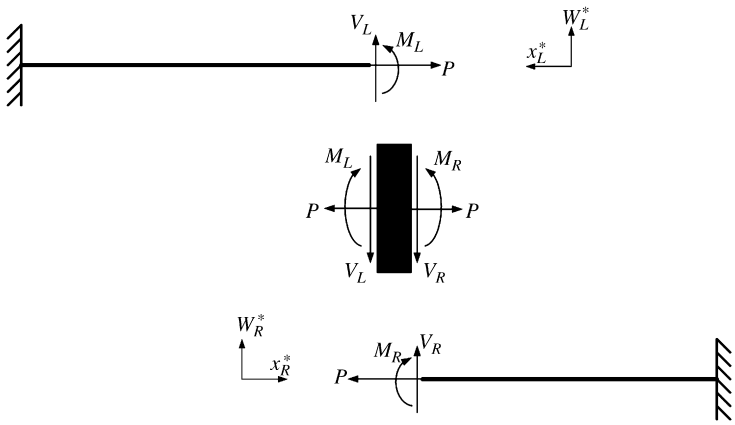

Fig. 3. The boundary conditions of the left and the right side beams, as well as the free body diagram of the lumped mass. The left side of the left beam and the right side of the right beam are built-in. Other ends are connected together through the lumped mass.

where

$$x_L = \frac{x_L^*}{L_L}, \quad t_L = \frac{t}{L_L^2}\sqrt{\frac{EI}{\rho A}}, \tag{3, 4}$$

$$P_L = \frac{PL_L^2}{2EI}, \quad W_L(x_L, t_L) = \frac{W_L^*(x_L^*, t)}{L_L}. \tag{5, 6}$$

For the right beam:

$$\frac{\partial^2 W_R}{\partial t_R^2} + \frac{\partial^4 W_R}{\partial x_R^4} - 2P_R\frac{\partial^2 W_R}{\partial x_R^2} = 0, \quad 0 \leqslant x_R \leqslant 1, \quad t_R \geqslant 0, \tag{7}$$

where

$$x_R = \frac{x_R^*}{L_R}, \quad t_R = \frac{t}{L_R^2}\sqrt{\frac{EI}{\rho A}}, \tag{8, 9}$$

$$P_R = \frac{PL_R^2}{2EI}, \quad W_R(x_R, t_R) = \frac{W_R^*(x_R^*, t)}{L_R}. \tag{10, 11}$$

One could use the method of the separation of variables to derive the general solution of the equation of motion for the left beam

$$W_L(x_L, t_L) = Y_L(x_L)T_L(t_L), \quad \text{where } Y_L(x_L) = \frac{Y_L^*(x_L^*)}{L_L}. \tag{12}$$

From which

$$\frac{\mathrm{d}^2 T_L}{\mathrm{d}t_L^2} + \Omega_L^2 T_L = 0, \tag{13}$$

$$\frac{\mathrm{d}^4 Y_L}{\mathrm{d}x_L^4} - 2P_L\frac{\mathrm{d}^2 Y_L}{\mathrm{d}x_L^2} - \Omega_L^2 Y_L = 0, \tag{14}$$

where

$$\Omega_L = \omega L_L^2\sqrt{\frac{\rho A}{EI}}. \tag{15}$$

The general solution of Eqs. (13) and (14) is of the form

$$T_L(t_L) = a_L \cos \Omega_L t_L + b_L \sin \Omega_L t_L, \tag{16}$$

$$Y_L(x_L) = c_1 \cos \lambda_L x_L + c_2 \sin \lambda_L x_L + c_3 \cosh \gamma_L x_L + c_4 \sinh \gamma_L x_L, \tag{17}$$

where

$$\lambda_L^2 = -P_L + \sqrt{P_L^2 + \Omega_L^2}, \quad \gamma_L^2 = P_L + \sqrt{P_L^2 + \Omega_L^2}. \tag{18, 19}$$

In a similar manner, for the right beam, we have

$$W_R(x_R, t_R) = Y_R(x_R)T_R(t_R), \quad \text{where } Y_R(x_R) = \frac{Y_R^*(x_R^*)}{L_R}, \tag{20}$$

$$\frac{\mathrm{d}^2 T_R}{\mathrm{d}t_R^2} + \Omega_R^2 T_R = 0, \tag{21}$$

$$\frac{d^4 Y_R}{dx_R^4} - 2P_R \frac{d^2 Y_R}{dx_R^2} - \Omega_R^2 Y_R = 0, \tag{22}$$

$$\Omega_R = \omega L_R^2 \sqrt{\frac{\rho A}{EI}}. \tag{23}$$

Moreover, the general solutions of Eqs. (21) and (22) are

$$T_R(t_R) = a_R \cos \Omega_R t_R + b_R \sin \Omega_R t_R, \tag{24}$$

$$Y_R(x_R) = c_5 \cos \lambda_R x_R + c_6 \sin \lambda_R x_R + c_7 \cosh \gamma_R x_R + c_8 \sinh \gamma_R x_R, \tag{25}$$

where

$$\lambda_R^2 = -P_R + \sqrt{P_R^2 + \Omega_R^2}, \quad \gamma_R^2 = P_R + \sqrt{P_R^2 + \Omega_R^2}. \tag{26, 27}$$

Using the spatial, Y's, and time, T's, functions, the boundary conditions can be expressed in the following form:

At the built-in ends:

at $x_L = 1$:

$$Y_L(x_L) = 0, \quad \frac{dY_L}{dx_L} = 0, \tag{28, 29}$$

at $x_R = 1$:

$$Y_R(x_R) = 0, \quad \frac{dY_R}{dx_R} = 0. \tag{30, 31}$$

At the location of the lumped mass $x_L = x_R = 0$:

$Y_L^* = Y_R^*$; consequently,

$$Y_L - \frac{1}{\beta} Y_R = 0, \tag{32}$$

$$\frac{dY_L^*}{dx_L^*} = -\frac{dY_R^*}{dx_R^*},$$

thus,

$$\frac{dY_L}{dx_L} + \frac{dY_R}{dx_R} = 0, \tag{33}$$

$$EI \frac{d^2 Y_L^*}{dx_L^{*2}} - EI \frac{d^2 Y_R^*}{dx_R^{*2}} = Mr^2 \omega^2 \frac{dY_L^*}{dx_L^*} = -Mr^2 \omega^2 \frac{dY_R^*}{dx_R^*},$$

so

$$\frac{d^2 Y_L}{dx_L^2} - \beta \frac{d^2 Y_R}{dx_R^2} = \alpha \delta^2 \Omega_L^2 \frac{dY_L}{dx_L}, \tag{34}$$

$$EI \frac{d^3 Y_L^*}{dx_L^{*3}} + EI \frac{d^3 Y_R^*}{dx_R^{*3}} = M\omega^2 Y_L^* = M\omega^2 Y_R^*,$$

accordingly,

$$\frac{d^3 Y_L}{dx_L^3} + \beta^2 \frac{d^3 Y_R}{dx_R^3} = \alpha \Omega_L^2 Y_L. \tag{35}$$

In Eqs. (32)–(35),

$$\beta = \frac{L_L}{L_R}, \quad \alpha = \frac{M}{\rho A L_L}, \quad \delta = \frac{r}{L_L}. \tag{36,37,38}$$

Substituting the general solutions of Eqs. (17) and (25) into Eqs. (28) through (35), the following homogeneous set of algebraic equations is obtained:

$$\begin{bmatrix}
\cos\lambda_L & \sin\lambda_L & \cosh\gamma_L & \sinh\gamma_L & 0 & 0 & 0 & 0 \\
-\lambda_L\sin\lambda_L & \lambda_L\cos\lambda_L & \gamma_L\sinh\gamma_L & \gamma_L\cosh\gamma_L & 0 & 0 & 0 & 0 \\
0 & 0 & 0 & 0 & \cos\lambda_R & \sin\lambda_R & \cosh\gamma_R & \sinh\gamma_R \\
0 & 0 & 0 & 0 & -\lambda_R\sin\lambda_R & \lambda_R\cos\lambda_R & \gamma_R\sinh\gamma_R & \gamma_R\cosh\gamma_R \\
1 & 0 & 1 & 0 & -\frac{1}{\beta} & 0 & -\frac{1}{\beta} & 0 \\
0 & \lambda_L & 0 & \gamma_L & 0 & \lambda_R & 0 & \gamma_R \\
-\lambda_L^2 & -\delta^2\alpha\Omega_L^2\lambda_L & \gamma_L^2 & -\delta^2\alpha\Omega_L^2\gamma_L & \beta\lambda_R^2 & 0 & -\beta\gamma_R^2 & 0 \\
-\alpha\Omega_L^2 & -\lambda_L^3 & -\alpha\Omega_L^2 & \gamma_L^3 & 0 & -\beta^2\lambda_R^3 & 0 & \beta^2\gamma_R^3
\end{bmatrix}$$

$$\times \begin{Bmatrix} c_1 \\ c_2 \\ c_3 \\ c_4 \\ c_5 \\ c_6 \\ c_7 \\ c_8 \end{Bmatrix} = \{0\}. \tag{39}$$

Eq. (39) has a trivial solution for c_1–c_8, unless the determinant of coefficients becomes zero for some specific values of λ_L, λ_R, γ_L, and γ_R, which are essentially functions of ω. The determinant of the dynamic matrix of Eq. (39) is the characteristic equation of the vibration of the uniform beam under the axial force with a lumped mass.

Besides the natural frequencies, Eq. (39) can be used to evaluate the mode shapes. By plotting the determinant of the dynamic matrix versus the natural frequencies, it can be deduced that every natural frequency of the beam is a simple root of the characteristic equation; so, assuming a non-zero value for one of the coefficients c_1–c_8, a reduced form of Eq. (39) will give the rest of the unknowns. Having a set of c's, one can make use of Eqs. (17) and (25) to find the mode shape related to that set.

3. Result and discussion

In this section, a set of dimensionless variables is introduced to represent oscillatory behavior of the system in a form easily comparable with the data reported in literature

$$\text{mass location}: \ \xi = \frac{L_L}{L_L + L_R},$$

$$\text{mass ratio}: \ \mu = \frac{M}{\rho A(L_L + L_R)},$$

$$\text{radius of gyration}: \ \eta = \frac{r}{L_L + L_R},$$

$$\text{axial force}: \ \sigma = \frac{P(L_L + L_R)^2}{2EI},$$

$$\text{natural frequency}: \ \Omega = \omega(L_L + L_R)^2\sqrt{\frac{\rho A}{EI}},$$

$$\text{dimensionless resonator's coordinate}: \ X = x^*/(L_1 + L_2), \ \text{where } x^* = x_2^* + L_1.$$

The quantity $\sqrt{\Omega}$ is frequently encountered in the published papers on vibration and is called frequency parameter. The first frequency parameter of the resonator, which corresponds to the first fundamental natural frequency, is plotted against the position of the rotary mass, ξ, and its radius of gyration, η, for a typical mass ratio, μ, as shown in Fig. 4. It can clearly be seen that the case of $\eta = 0$ corresponds to the lumped mass model with no rotary inertia, and is the lower bound of the natural frequencies. This curve is in full agreement with the previous published works [2,3] in which, the rotary inertia of the lumped mass is neglected. In addition, when the mass is attached at the positions with no rotation ($\xi = 0$ or 0.5), the frequency parameters converge to that of the no rotary inertia.

The case of $\eta \to \infty$ is adopted from Ref. [12] in which, the lumped mass is assumed to be laterally guided. The second frequency parameter of the resonator versus the position and the radius of gyration of the mass for a typical mass ratio is shown in Fig. 5. It can be seen that the special case of $\eta = 0$ is the lower bound of the frequency parameter as it is in the first mode. Moreover, for the cases of $\eta = 1$ and 2 they are hardly noticeable. It is worth noting that, the frequency parameter, for each curve, has a maximum value when the rotary lumped mass is located at the mid-point of the beam, which corresponds to the point with the maximum rotation at this mode.

A similar phenomenon has occurred in Fig. 6, in which the third frequency parameter is plotted as a function of the mass position and the radius of gyration for a same mass ratio as before. It is evident that the frequency parameter has maximum where there is a node at the position of the rotary mass, and it approaches to the case of $\eta = 0$, where the mode shape has zero slope. Moreover, it can be seen that the different curves corresponding to the different radii of gyration approach to an imaginary upper bound curve, which corresponds to the case when η approaches infinity.

One could investigate this effect further in more detail for which, the first, second, and the third frequency parameters of the resonator are plotted in Figs. 7–9, respectively, as functions of the radius of gyration and the

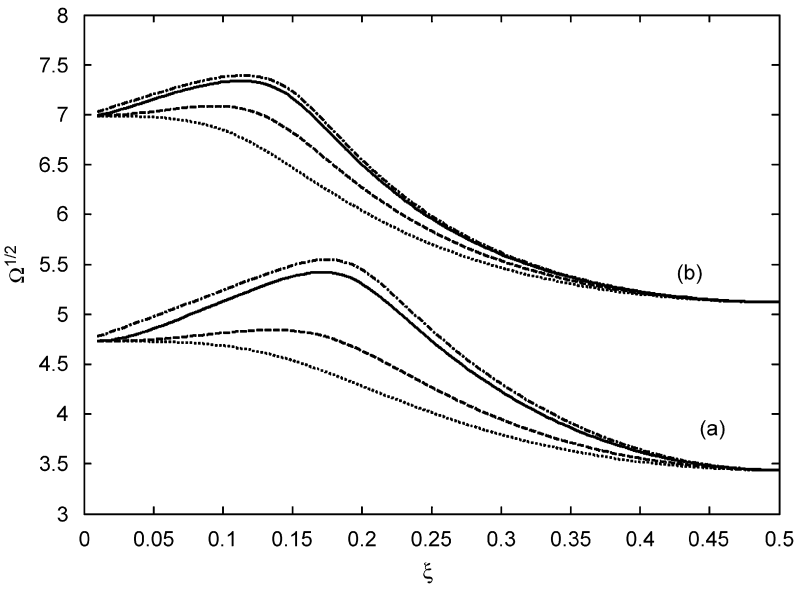

Fig. 4. First frequency parameter of resonator vs. the position of rotary mass, ξ, for $\mu = 1$: $\eta = 0$ (..), $\eta = 0.1$ (- -), $\eta = 1$ (solid), $\eta \to \infty$ (-.), for (a) $\sigma = 0$ and (b) $\sigma = 81$.

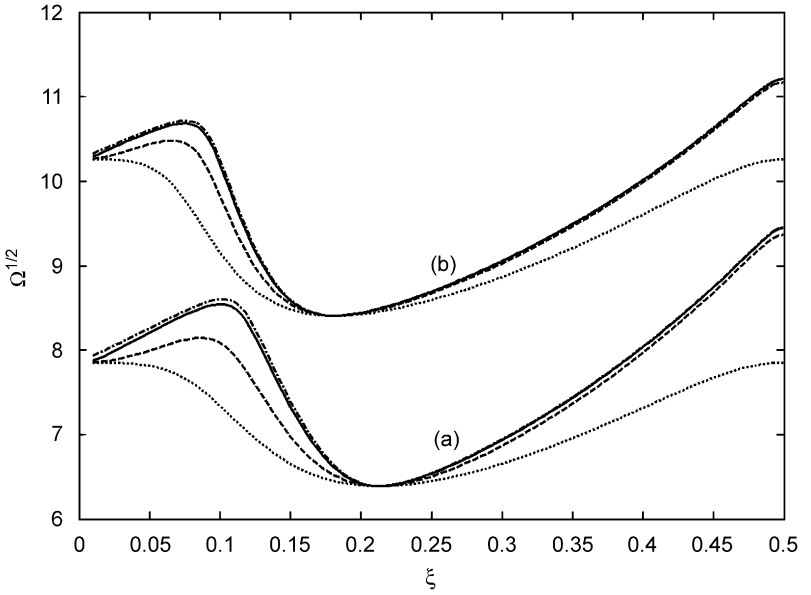

Fig. 5. Second frequency parameter of resonator vs. the position of rotary mass, ξ, for $\mu = 1$: $\eta = 0$ (..), $\eta = 0.1$ (- -), $\eta = 1$ (solid), $\eta \to \infty$ (-.), for (a) $\sigma = 0$ and (b) $\sigma = 81$.

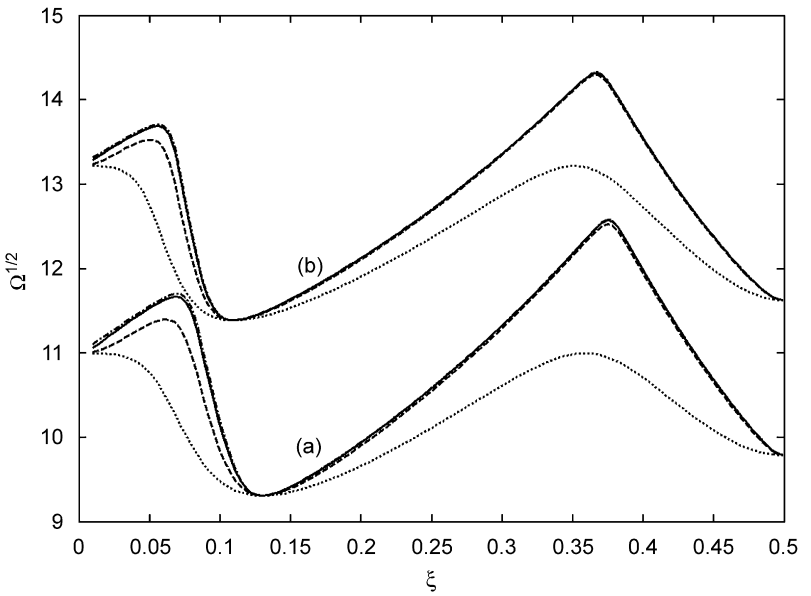

Fig. 6. Third frequency parameter of resonator vs. the position of rotary mass, ξ, for $\mu = 1$: $\eta = 0$ (..), $\eta = 0.1$ (- -), $\eta = 1$ (solid), $\eta \to \infty$ (-.), for (a) $\sigma = 0$ and (b) $\sigma = 81$.

mass ratio. In each figure, the mass location is chosen from Figs. 4–6, respectively, to achieve the maximum gradient of the frequency parameter. It can be seen that the curves of the frequency parameters show asymptotic behavior. As can be seen from Figs. 7–9, the asymptote, in each family of curves, corresponds to the frequency parameter of a beam with a guided mass of the same mass ratio and position [12]. This also justifies the increase in the natural frequency upon the inclusion of the rotary inertia to the model, since a

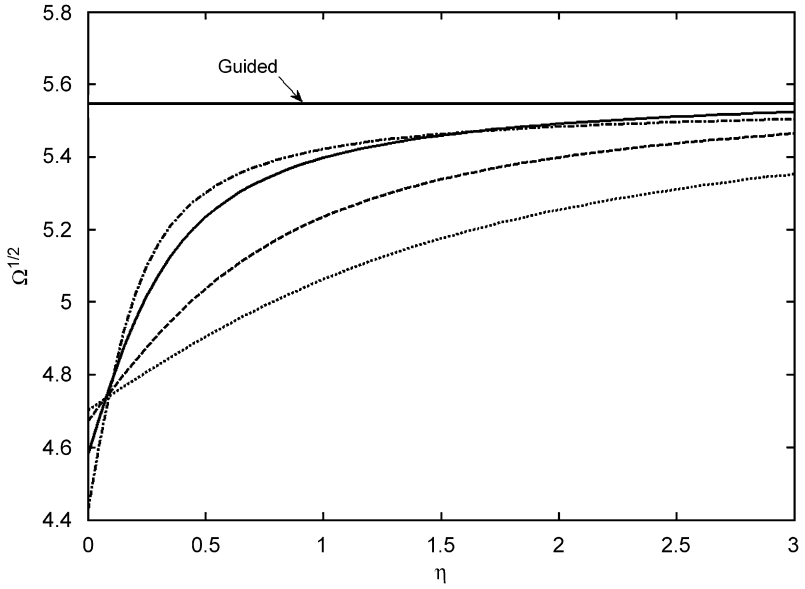

Fig. 7. First frequency parameter vs. radius of gyration, η, for $\xi = 0.17$: $\mu = 0.1$(..), $\mu = 0.2$ (- -), $\mu = 0.5$ (solid), $\mu = 1$ (-.).

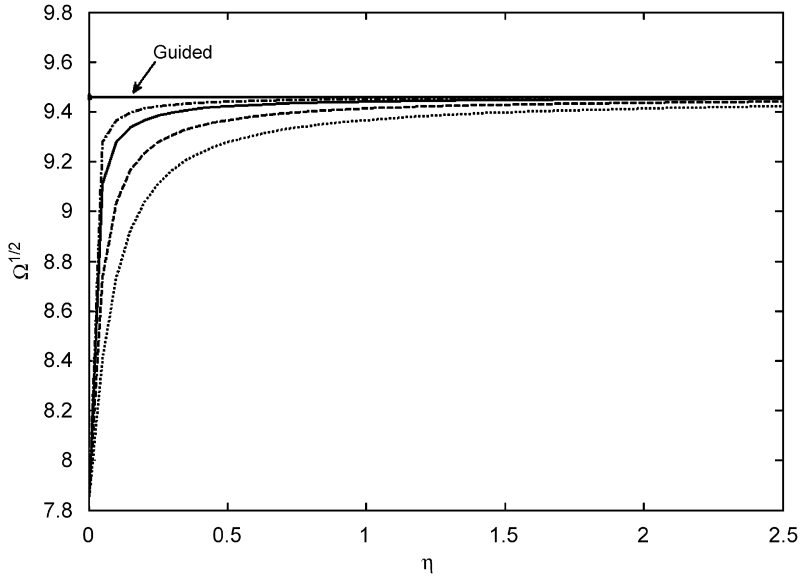

Fig. 8. Second frequency parameter vs. radius of gyration, η, for $\xi = 0.5$: $\mu = 0.1$(..), $\mu = 0.2$ (- -), $\mu = 0.5$ (solid), $\mu = 1$ (-.).

guided mass separates the beam into two shorter beams with a higher rigidity, and hence increases the natural frequency.

Fig. 10 shows the first frequency parameter versus the mass location and ratio for a typical value of the radius of gyration. It can be seen that for a given radius of gyration, a lower mass ratio does not necessarily results into a higher natural frequency, but it depends on the mass location too.

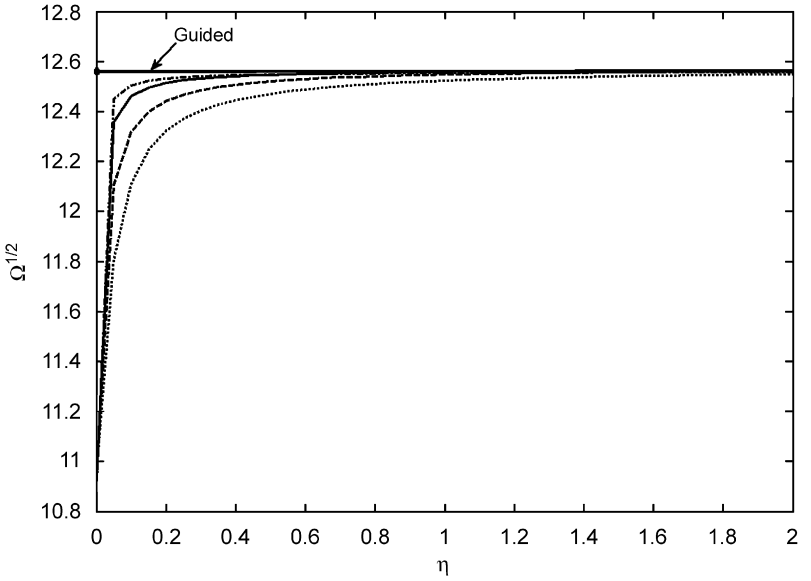

Fig. 9. Third frequency parameter vs. radius of gyration, η, for $\xi = 0.38$: $\mu = 0.1$ (..), $\mu = 0.2$ (- -), $\mu = 0.5$ (solid), $\mu = 1$ (-.).

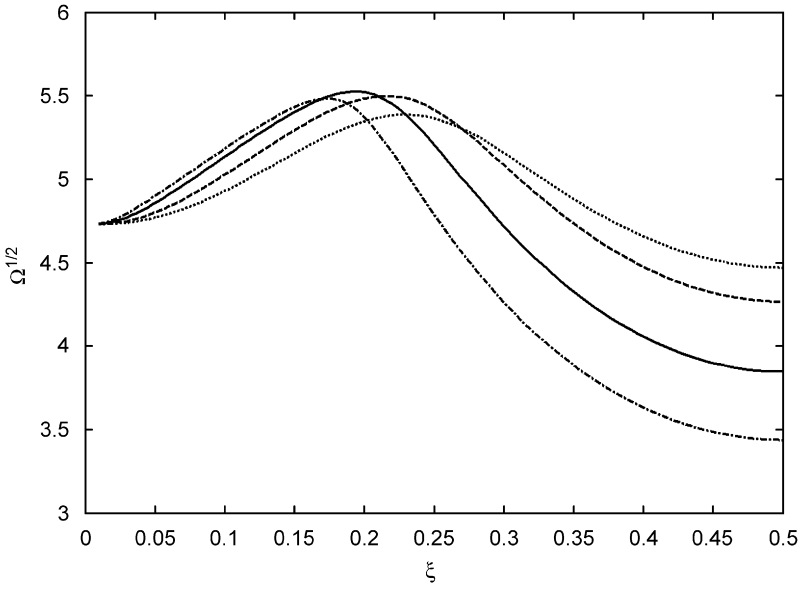

Fig. 10. First frequency parameter vs. mass location, ξ, for $\eta = 2$: $\mu = 0.1$ (..), $\mu = 0.2$ (- -), $\mu = 0.5$ (solid), $\mu = 1$ (-.).

For instance, when $\xi < 0.16$, resonators with higher mass ratios exhibit higher natural frequencies at the first mode of vibration. A similar effect can be seen in Figs. 11 and 12 in which, the second and the third frequency parameters are plotted.

Fig. 13 depicts the first frequency parameter of the resonator versus the axial force for various sets of the mass locations, ratios, and the radii of gyration, compared to the cases of the clamped–clamped beam and the beam with the guided mass. This figure shows that depending on the mass location, ratio, and the radius of gyration, the natural frequency of the resonator may be even more than the corresponding clamped–clamped

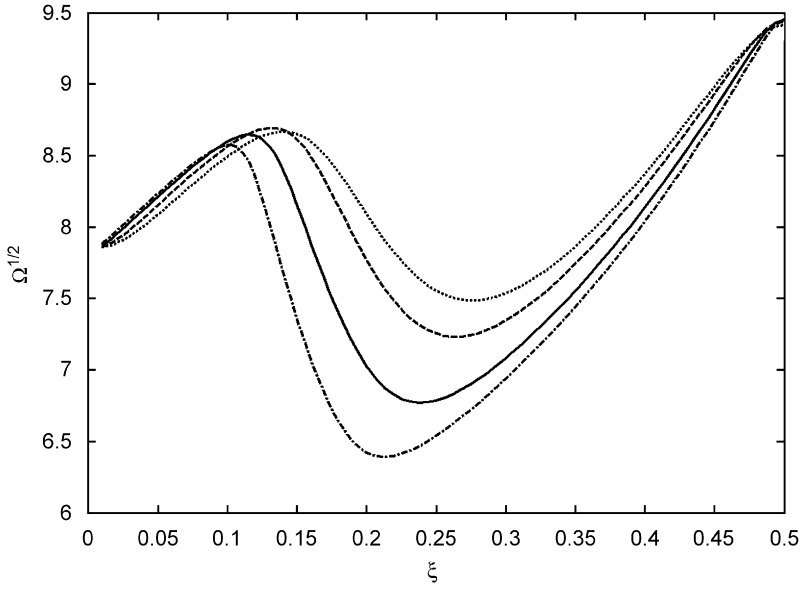

Fig. 11. Second frequency parameter vs. mass location, ξ, for $\eta = 2$: $\mu = 0.1$ (..), $\mu = 0.2$ (- -), $\mu = 0.5$ (solid), $\mu = 1$ (-.).

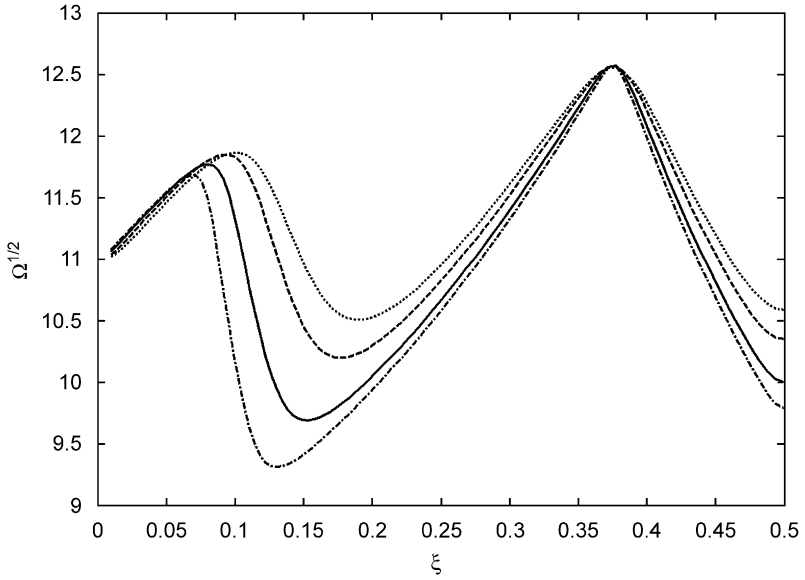

Fig. 12. Third frequency parameter vs. mass location, ξ, for $\eta = 2$: $\mu = 0.1$ (..), $\mu = 0.2$ (- -), $\mu = 0.5$ (solid), $\mu = 1$ (-.).

beam. This conclusion is important in the design of a MEMS-based resonator, in which the designer has to decide on the mechanism of excitation of the resonator and the detection of its oscillations.

As pointed out before, one is able to derive the mode shapes by using Eqs. (17), (25), and (39). The first two mode shapes for a set of parameters $\sigma = 0$, $\xi = 0.5$, $\mu = 6$, and $\eta = 0.6$ presented in Fig. 14, which confirm the influence of the mass rotary inertia and the location on the frequency parameter. It can be seen that the beam has a smaller slope at its mid-point compared to the case with no rotary mass [2].

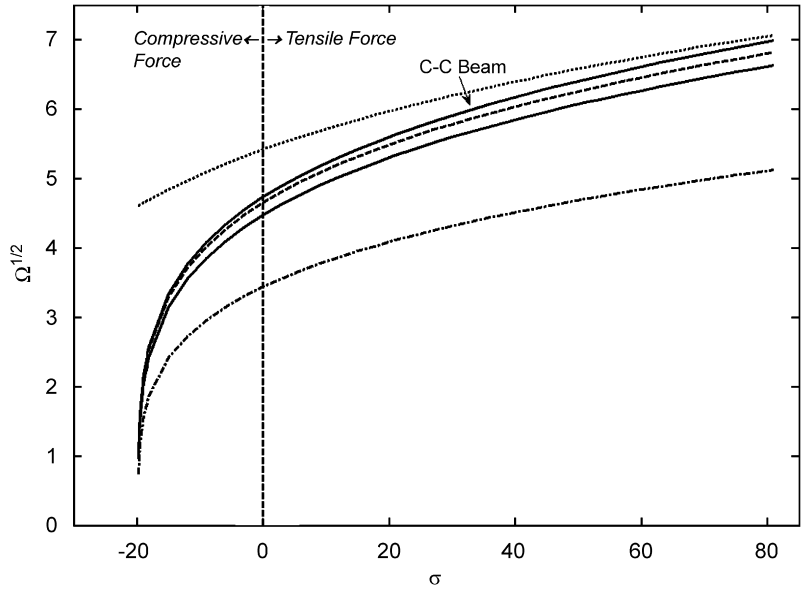

Fig. 13. First frequency parameter of resonator vs. axial force, σ, for $\xi = 0.5$, $\mu = 0.1$, $\eta = 0.5$ (-.), $\xi = 0.5$, $\mu = 0.1$, $\eta = 0.1$ (solid), $\xi = 0.3$, $\mu = 0.1$, $\eta = 0.1$ (- -), guided beam $\xi = 0.3$, $\mu = 0.1$ (..), and clamped–clamped beam.

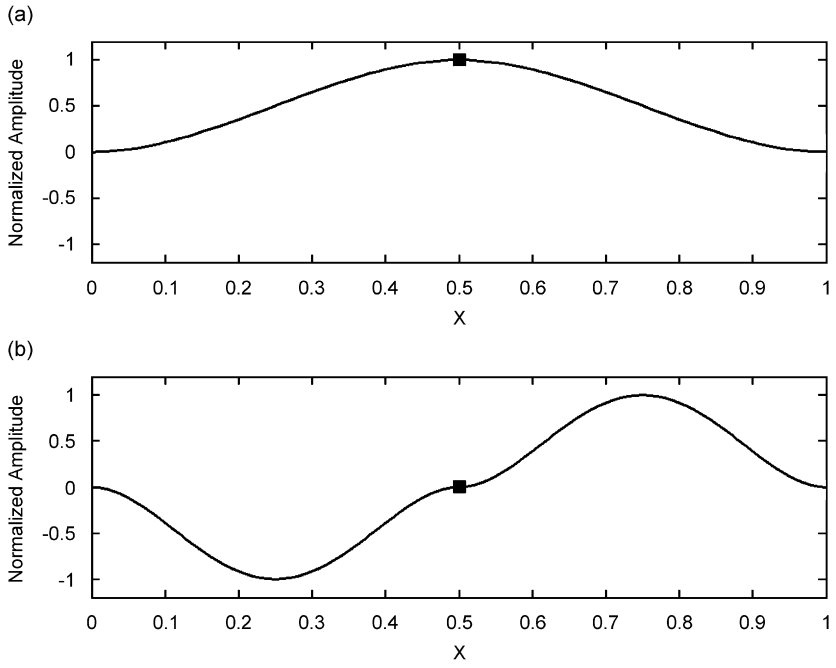

Fig. 14. First (a) and second (b) mode shapes of a beam with parameters $\sigma = 0$, $\xi = 0.5$, $\mu = 6$, and $\eta = 0.6$. Mode shapes are normalized to have the maximum displacement equal to one unit. Solid rectangle represents the lumped mass.

The mode shapes of a non-symmetric beam with parameters $\sigma = 0$, $\xi = 0.2$, $\mu = 0.6$, and $\eta = 0.13$ are illustrated in Fig. 15. As expected, at the location of the lumped mass, the beam has less amplitude than the corresponding point on the other half of the beam. The significance of this figure is that it gives the designer an

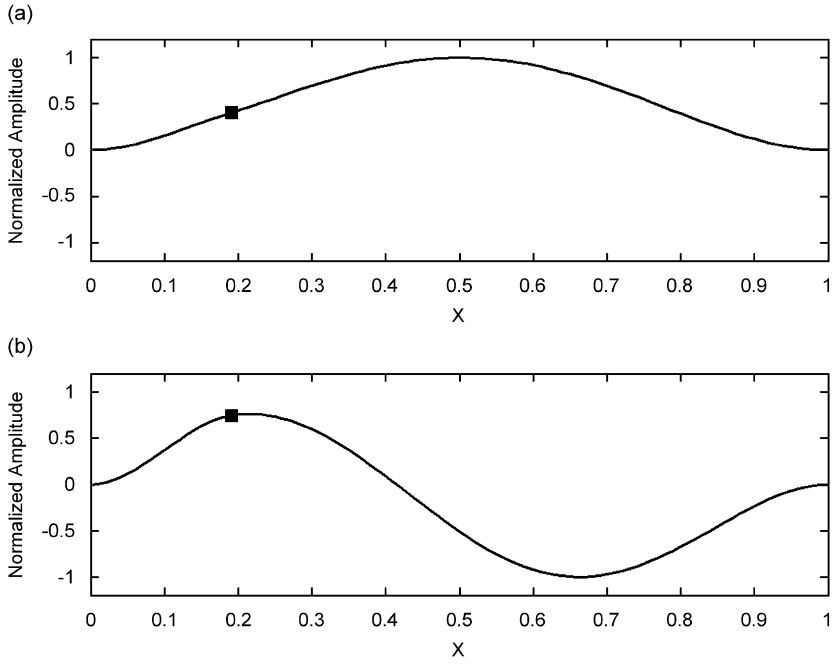

Fig. 15. First (a) and second (b) mode shapes of a beam with parameters $\sigma = 0$, $\xi = 0.2$, $\mu = 0.6$, and $\eta = 0.13$. Mode shapes are normalized to have the maximum displacement equal to one unit. Solid rectangle represents the lumped mass.

insight idea as how the rotary inertia can be used to extend the stability region of operation of the resonator by reducing the rotation of the comb-drive.

4. Conclusion

Need for the exact solution of the oscillatory behavior of a beam with a lumped mass within its interval under an axial force is encountered in the study of double-ended tuning fork (DETF) used as resonator structure in micro-machined devices. In this paper, the beam is treated as two beams connected to each other through the lumped mass and the characteristic equation is derived from the governing equations of motion of the two beams. It has been shown that higher natural frequencies than the case with a lighter mass can be achieved by proper placement of the lumped mass. It is found that in some cases, the concentrated mass has no influence on the specific natural frequencies of the beam. During the design of a DETF, one must be aware of the interaction that exist between different design parameters. The approach in this paper is capable to determine the exact mode shapes of vibrations that are inevitably required in the study of the system in the time-domain, as well as the stability of electrostatic exciter/detector.

References

[1] X. Sun, R. Horowitz, K. Komvopoulos, Stability and resolution analysis of a phase-locked loop natural frequency tracking system for MEMS fatigue testing, *ASME Transactions, Journal of Dynamic Systems, Measurement and Control* 124 (2002) 599–605.

[2] P.A. Hassanpour, W.L. Cleghorn, E. Esmailzadeh, J.K. Mills, Exact solution of the oscillatory behavior of a beam with a concentrated mass within its interval under axial force, *Journal of Vibrations and Control* (2007), in press.

[3] G.B. Chai, K.H. Low, On the natural frequencies of beams carrying a concentrated mass, *Journal of Sound and Vibration* 160 (1993) 161–166.

[4] K.H. Low, G.B. Chai, Experimental and analytical investigations of vibration frequencies for center-loaded beams, *Computers and Structures* 48 (1993) 1157–1162.

[5] K.H. Low, Equivalent-center method for quick frequency analysis of beams carrying a concentrated mass, *Computers and Structures* 50 (1994) 409–419.

[6] M.A. De Rosa, C. Franciosi, M.J. Maurizi, On the dynamic behavior of slender beams with elastic ends carrying a concentrated mass, *Computers and Structures* 58 (1996) 1145–1159.
[7] S. Naguleswaran, Lateral vibration of a uniform Euler–Bernoulli beam carrying a particle at an intermediate point, *Journal of Sound and Vibration* 227 (1999) 205–214.
[8] M. Skrinar, On elastic beams parameter identification using eigenfrequencies changes and the method of added mass, *Computational Materials Science* 25 (2002) 207–217.
[9] I.G. Currie, W.L. Cleghorn, Free lateral vibrations of a beam under tension with a concentrated mass at the mid-point, *Journal of Sound and Vibration* 123 (1988) 55–61.
[10] S.M. Wiedemann, Natural frequencies and mode shapes of arbitrary beam structures with arbitrary boundary conditions, *Journal of Sound and Vibration* 300 (2007) 280–291.
[11] P.A. Hassanpour, W.L. Cleghorn, E. Esmailzadeh, J.K. Mills, Modeling and analysis of a resonant sensor actuated by a bent beam thermal actuator, *Proceedings of the 17th IASTED International Conference on Modeling and Simulation*, Montreal, Quebec, Canada, May 24–26, 2006.
[12] P.A. Hassanpour, W.L. Cleghorn, E. Esmailzadeh, J.K. Mills, Exact solution of the oscillatory behavior of a beam with a guided mass within its interval under axial force, *Proceedings of CANCAM 2007*, Toronto, Canada, June 3–7, 2007.
[13] G. Zhou, D. Low, P. Dowd, Method to achieve large displacements using comb-drive actuators, *Proceedings of SPIE-The International Society for Optical Engineering* 4557 (2001) 428–435.
[14] S.S. Rao, *Mechanical Vibrations*, Pearson Prentice-Hall, Upper Saddle River, NJ, 2004.